Transient degassing events at the lava lake of Erebus volcano, Antarctica: Chemistry and mechanisms

Tehnuka Ilanko [a],[*], Clive Oppenheimer [a], Alain Burgisser [b],[c], Philip Kyle [d]

[a] Department of Geography, Cambridge University, Downing Place, Cambridge CB2 3EN, UK
[b] CNRS, ISTerre, F-73376 Le Bourget du Lac, France
[c] Université Savoie Mont Blanc, ISTerre, F-73376 Le Bourget du Lac, France
[d] Department of Earth & Environmental Science, New Mexico Institute of Mining & Technology, Socorro NM87801, USA

ARTICLE INFO

ABSTRACT

We report here on the chemical signature of degassing at Erebus lava lake associated with intermittent explosions and the return to passive conditions. Explosions caused by bubble bursts were frequent during the 2013 field season, providing the first opportunity to observe such activity since 2005–06. Several of the explosions were captured by multiple instruments including an open-path Fourier transform infrared spectrometer. Explosive bubble bursts and other transient degassing events are associated with gas compositions that are distinct from the usual range of passive degassing compositions. We set out to compare the chemical signature of explosive degassing during the 2005–06 and 2013 episodes, and to characterise the chemistry of gases emitted during the period of lake refilling after explosions. We found little change in the explosive gas chemistry between 2005–06 and 2013, suggesting reactivation of a common mechanism of gas segregation. Bubbles can be distinguished by their size and composition, the ranges of which are likely modified during ascent by gas–melt interaction and adiabatic expansion. The proportions of water, SO_2, and HCl in the emitted gas plume increase during the refill of the lake after explosions, as the lake is recharged by a combination of magma that has already partially degassed, and that vesiculates rapidly in response to the drop in magmastatic pressure at the lake.

© 2015 The Authors. Published by Elsevier Ltd. This is an open access article under the CC BY license (http://creativecommons.org/licenses/by/4.0/).

1. Introduction

Explosions at the surface of the Erebus lava lake, Antarctica, occur sporadically and range considerably in magnitude. They result from gas bubbles or slugs bursting at the surface of the lava lake. These vary from small (a few metres in diameter) bubbles that rupture without generating bombs, to overpressured bubbles that expand to the lake diameter prior to rupture, sometimes ejecting bombs a few hundred metres over the summit crater rim. The largest explosions leave the lake empty, and camera observations show the lake refilling over the following minutes (e.g. [10]). The frequency of explosions is variable – smaller events are commonly observed, whereas the large, lake evacuating events occur in episodes of several months' duration, during which there can be several explosions per day. The 2005 and 2013 field seasons, each lasting 4–5 weeks in the austral summers, coincided with two such episodes. Explosions were captured regularly by thermal infrared cameras and seismometers, and in the 2005 season the physical parameters of these explosions were studied by Gerst [12] and

Gerst et al. [13,14] using Doppler radar. A number of infrasound studies have also been carried out on explosions both during and between episodes of increased activity (e.g. [36,21]). Between explosions, the lake appears to return to a stable passive degassing regime similar to that seen in other years, including exhibiting cyclic changes in thermal radiance [34] and degassing.

Bombs expelled beyond the crater rim during explosions have provided detailed geochemical and petrological information about the phonolite magma (e.g. [23]). The chemistry of gas released from bursting bubbles can also be measured by Fourier Transform infrared (FTIR) spectrometers operating at high time resolution (up to 1 Hz). Measurements are available for the period leading up to a bubble entering the lake, for the gas released from the bubble, and, in the cases of larger explosions that drain the lake, during refill and resumption of passive degassing.

Gas emissions associated with large explosions in 2005–06 were considered by Oppenheimer et al. [30] in the context of the deeper plumbing system at Erebus. Compositionally, these were found to be distinct from passive degassing in having high CO_2/CO and CO_2/H_2O. Burgisser et al. [6] used these same explosion compositions for thermodynamic modelling of the potential

* Corresponding author.

sources of large bubbles. However, the refill of the lake has not been studied before, and is of particular interest because of the information it could reveal about the convective regime in the lake and inferred exchange flow in the subjacent conduit, since magma ascent rates likely increase by an order of magnitude in the transition from bidirectional to unidirectional conduit flow. Analysis of FTIR spectroscopic data and infrared camera imagery for the 2013 field season has revealed consistently clear cycles [34], making it especially suitable for studying the return to passive degassing. The dataset also enables the first gas geochemical comparison to be made with the 2005 explosions.

Here, we use the seven gas species (H_2O, CO_2, SO_2, CO, HF, HCl, OCS) for which pathlength measurements were obtained using FTIR spectroscopy, to characterise plume gas compositions during and after explosions. Our key objectives are (i) to describe the compositions of explosion gas from 2013, and compare with observations from 2005 to 06; (ii) to characterise gas compositions of smaller bubble bursts and other transient degassing events for comparison with the explosions and with the passive degassing signature; and (iii) to characterise the temporal evolution of the gas chemistry as the lake refills. We then consider the implications of our findings for the dynamics of magma supply and degassing at Erebus.

2. Methods

Only brief outlines of methods of data collection and processing are given here. Detailed explanations are available elsewhere as referenced below. Further information is given in Supplementary Materials.

2.1. Collection and pre-processing of FTIR spectra

Spectra used in this study were acquired over about two weeks in December 2013. Data collection procedures were similar to those described by Oppenheimer and Kyle [28]. A MIDAC spectrometer was set up at Shackleton's Cairn, on the western side of the summit crater. A liquid nitrogen-cooled indium-antimonide detector was used, sometimes with a 10-inch Newtonian telescope with a specified field of view of 3 mrad corresponding to a footprint on the lake of order 1 m. The acquisition rate for interferograms averaged about 0.6 Hz and successive scans were not co-added, to obtain the best possible temporal resolution. Interferograms were subsequently converted to single beam spectra with the software used for data collection, AutoQuant Pro. All spectra in this study were collected using the lava lake surface, at a distance of approximately 300 m, as the infrared source. The lake area during this time was approx. 580 m^2 [33].

2.2. Bubble identification

Large explosions (i.e. those from lake-size bubbles) were identified using thermal imagery recorded by a camera at the same site as the FTIR spectrometer, and by inspection of seismograms. Infrared images from the thermal camera show explosions and, in some cases, the emptying and refill of the lake. Explosion signals can also be identified in seismograms recorded at various sites including Nausea Knob, E1S, Lower Erebus Hut, and Truncated Cones [3]. The large explosions presented in Table 2 were all identified in seismic data and/or infrared images. Due to the vagaries of timekeeping on Erebus, the FTIR measurements are not precisely synchronised with the infrared imagery and seismic signals, but there is a significant increase in the intensity of FTIR spectra during explosions, so that the start of an explosion can be easily identified.

Of the large bubbles identified in infrared images and/or seismic data in the 2013 field season, FTIR data of usable quality were available for 25 bubbles, observed from 4 to 15 December 2013. Other bubble bursts were apparent in the seismic record but were not recorded by FTIR spectroscopy owing to intermissions in data acquisition, or were not evident in FTIR spectra (e.g. due to thick fumes in the crater and low IR signal). Minor changes to gas ratios from smaller events cannot be systematically isolated from the variation that occurs during passive degassing although, in a few cases, small (metre-scale) bubbles are apparent as instantaneous changes in gas ratios, and verifiable in infrared images or seismograms.

2.3. Gas retrievals and modelling

Retrievals followed methods described by Oppenheimer and Kyle [28]. To correct for background water and CO_2 in passive degassing, we assume that atmospheric CO is negligible, and calculate intercepts from scatter plots of H_2O and CO_2 column amounts (CAs) against CO before each explosion. These intercepts are taken to be the atmospheric H_2O and CO_2 CAs during passive degassing, and subtracted from all retrievals of these gases. Gas ratios for explosions, however, are based on linear regressions through scatter plots of the two gases without background corrections, using data points spanning the first seconds of the explosion. Retrievals were carried out for FTIR data collected in 2005 following the same procedures as for the 2013 data.

The FTIR spectra and retrievals for large bubbles may be less accurate than those for passive degassing, for a number of reasons: (i) measurements use the lava lake as a source, so the IR signal is affected by increased radiance as the bubble bursts, followed by a decrease if the lake is emptied, at which time there is also lower thermal contrast between the gas and the lava lake radiation source; (ii) the bubble burst is associated with high amounts of gas that may fully absorb the source radiation; (iii) measurements immediately after the bubble may not be entirely associated with refilling, if a significant proportion of gas from the explosion is still present in the crater; and (iv) as a result of the changing conditions, unlike the passive degassing regime in which gas temperatures and pressures are relatively stable between spectra, the optimal temperature and pressure for retrieval may also change significantly. Consequently, retrieval errors and uncertainty are higher during, and in the seconds immediately after, an explosion (see Supplementary Materials).

We have determined equilibrium temperatures (T_{eqm}), calculated at local atmospheric pressure, for the explosions using the thermodynamic model D-Compress, following Burgisser et al. [6] and using gas ratios (CO_2/CO, CO_2/H_2O, CO_2/SO_2, SO_2/OCS, CO_2/HCl) derived from FTIR spectra.

3. Results

We classify bubbles and other transient degassing events into broad groups as follows based on the infrared imagery (Fig. 1) and retrieved gas ratios (n indicates the number of events recorded in each class in Dec. 2013):

(i) **Violent explosions (n = 13).** The lake is mostly emptied and bombs are likely to be thrown over the summit crater rim. The degree of fragmentation (i.e. the size of pyroclasts) visible in infrared images is variable, as is the direction of the bubble membrane rupture indicated by the trajectories of pyroclasts. The images suggest a range of rise speeds or overpressures; in particular, we observe both spherical cap bubbles that are slower to expand, fill the entire lake before rupture, and generate larger fragments, and explosions with
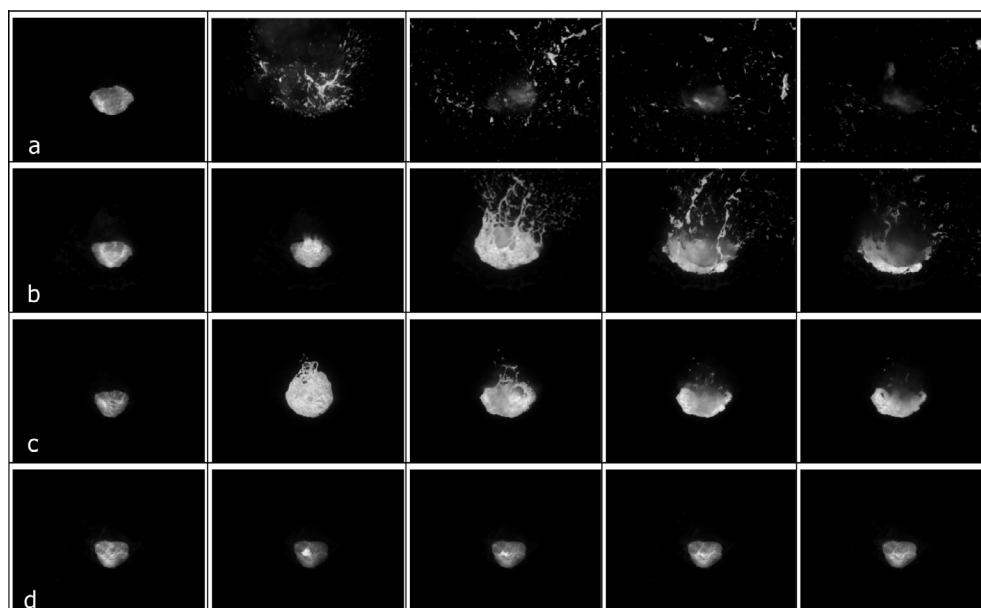
Fig. 1. Infrared images of explosions at (a) 04:30 07/12/13; (b) 06:54 04/12/14; (c) 05:00 10/12/13; (d) 02:51 11/12/13; (UTC) at sampling intervals of approximately 2 s. These depict bubbles of classes (i)–(iv) respectively, with (d) showing a small, non-explosive bubble.

greater overpressure where the bubble is not clearly visible but rupture is rapid, producing smaller fragments (i.e. a higher proportion of ash) with a jet-like dispersal of pyroclasts. These may correspond to the type I and II bubble categories described by Gerst [12] and Gerst et al. [13] in 2005–06. Type I bubbles have a longer period of expansion before bursting, while type II bubbles burst earlier, with higher velocities and acceleration. Mah [25] and Aster et al. [4] also categorise explosion observations by their seismic (VLP) signals: Group 1 explosions have the form of jets, and Group 2 explosions are from the slower onset bubbles; however, their post-eruption codas are very similar [4]. In our classification, class (i) explosions are distinct from other classes in that they are normally observed during episodes of increased activity lasting several months, such as in 2013–14, 2005–06, and previously in 1984–88 [10].

(ii) **Minor explosions ($n = 9$).** These are usually associated with rupture of spherical cap bubbles, but could include jets. They are tens of metres in diameter, typically filling the lake. The bombs produced stay within the Main Crater and land on the sides of the Inner Crater or return to the lake. The lake is not completely emptied. This class of explosions is not restricted to periods of increased explosive activity.

(iii) **Large bubbles ($n = 3$).** Bubbles have diameters up to tens of metres; they may not fill the lake and often collapse inwards, generating few or no bombs. The lake level does not appear to be much affected. The smallest bubbles are associated with minor seismic signals, and changes in gas ratios are also minor, so similar events may exist in FTIR and infrared data without being identified here.

(iv) **Small bubbles ($n = 4$) and other degassing events ($n = 7$).** Two further types of changes are evident in gas ratios. One group is characterised by high proportions of OCS in the emitted gas and a longer duration (several minutes) with no obvious change apparent in thermal images. The other group represents cracks in the lake crust or small bubbles, up to a few metres in diameter, that release gas non-explosively. Small bubbles are often difficult to detect in FTIR data, as the associated changes in gas ratios can be within the normal range of gas ratios measured during passive degassing.

These classes suggest a spectrum, within transient degassing events, of affected lake surface area, explosion energy, and emitted gas volume decreasing from class (i) to (iv). Our classification (Table 1) has similarities to explosions described by Gerst [12] and Aster et al. [4]: class (i) and (ii) both include explosions that resemble type I/Group 2 and type II/Group 1, and the definitions for class (iii) explosions and bubbles in class (iv) may overlap with *small* type explosions [12], wherein the surface membrane of the bubble does not rupture, or has a delayed rupture. Tazieff [38] described a similarly non-explosive, silent formation and collapse of a large bubble at Erebus lava lake in the 1970s, which possibly fits the class (iii) description. However, it was the only such event

Table 1
Overview of degassing events by class, indicating possible overlaps with classifications by Dibble et al. [10] and Gerst [12] from visual, and by Aster et al. [4] from seismic, observations.

Class	Description	Dibble et al. [10]	Type [12] and Group [4]
i	*Violent explosions:* Type I bubbles fill lake diameter; bombs thrown beyond Main Crater rim	'Strong'	Type I/Group 2 and type II/Group 1
ii	*Minor explosions:* Type I bubbles fill lake diameter; bombs remain within Main Crater	'Medium' & 'Strong'	Mainly type I/Group 2; some type II/Group I
iii	*Large bubbles:* Bubbles are tens of metres in diameter; few bombs, landing mainly within lake	'Weak' & 'Medium'	Type I/Group 2 and *small* type
iv	*Small bubbles:* Bubbles are up to a few metres in diameter; no explosion	'Weak'	Include some *small* type
	Other degassing events: No visible changes	NA	NA

observed at the time. Various bubble sizes and explosion styles were also observed in the 1986–88 field seasons, by Dibble et al. [10], who describe 'strong' explosions producing ash and bombs, 'medium' explosions that produce only bombs, and 'weak' ones that involve a bubble forming and collapsing without producing bombs. This spectrum thus appears to be characteristic of Erebus.

We report first (Section 3.1) the compositions of explosions (i.e. class (i)–(iii) bubbles) in 2013, describing the change in gas ratios through the onset of the explosion to the compositions of the bubbles themselves. This section includes a comparison to explosions from 2005 to 06. Other transient events (class (iv) events) are reported in Section 3.2, and the refill period after large explosions is described in Section 3.3.

3.1. Explosion compositions

We considered the changing compositions of gas emitted during the onset of the explosions and during lake refill, using time-series plots of gas CAs and gas ratios (Fig. 2) and scatter plots for gas pairs (Fig. 3). The compositions of explosions and other degassing anomalies, in terms of selected gas ratios, are presented in Tables 2 and 3.

3.1.1. Bubble compositions

The compositions of 25 class (i) to (iii) bubbles measured in 2013, along with their bubble classification and equilibrium temperatures (T_{eqm}) calculated at 0.61 bars using D-Compress, are shown in Table 2. The gas released by large bubbles is richer in CO_2, CO, and OCS. The CO_2/CO ratios during large explosions are about 3–6 times those measured during passive degassing (e.g. Fig. 2b), while CO_2/H_2O reaches 2–10 times passive degassing levels (Fig. 2d). Generally, there is also an increase in CO_2/SO_2 and CO_2/HCl ratios (Fig. 2c), while SO_2/OCS drops by a factor of 5–10 (Fig. 2d). For class (iii) bubble bursts in which most of the disrupted magma lands in the lava lake, CO_2/CO ratios are comparable to those in class (i) and (ii) large bomb-throwing explosions, but the gas appears richer in H_2O, SO_2, and HCl, and contains less CO_2, CO, and OCS.

Fig. 3 shows the evolution of gas ratios through a bubble burst and lake refill. Although the primary features of the explosions are sharp increases in CO_2 and OCS, there are also marked, if delayed, increases in SO_2/HCl, SO_2/H_2O, HCl/HF, and HCl/H_2O. The CAs of OCS show a sharp increase, followed by a slower decrease to normal or below-normal levels, before the level of SO_2 begins to drop. This suggests that most OCS is released from the bubble burst, while a significant proportion of SO_2 associated with explosions is degassed from the spatter, or rapidly emitted through the remnants of the lake following the explosion.

Calculations of fO_2 based on T_{eqm} and CO_2/CO ratio show that explosions are at $\Delta NNO = -0.81$ to -1.2 (Table 2), whereas passive degassing and pre-explosion compositions are around $\Delta NNO = -1.5$.

3.1.2. Comparison to 2005–06 explosions

Compositions of class (i)–(iii) explosions are similar to those from explosions in the 2005 field season, as shown in Fig. 4, although CO_2/CO is somewhat higher for the explosions in 2013. However, this could be because ratios are calculated using linear regressions through just a few data points. The higher level of uncertainty in retrievals for explosions could account for further discrepancies, as could the size of explosions, since 2005–06 bubble sizes were not analysed. Note that results for the 2005 spectra differ significantly from those in Oppenheimer et al. [30], reflecting possible differences in how ratios were calculated, updates to the HITRAN molecular spectroscopic database, and choice of retrieval

parameters. A comparison of available equilibrium temperatures shows that the updated compositions affect these by up to 15%. Further ratios for 2005 are given in the Supplementary Materials.

3.2. Class (iv) degassing events

Some explosions are associated with a second peak in gas ratios within a minute of the first peak. The 14 December 2013 16:38 explosion is especially clear in thermal infrared (TIR) images, showing the lava lake for about 25 s following the eruption. Within about 10 s another large quantity of gas is emitted, obscuring the lake. This gas has elevated CO_2/CO and CO_2/SO_2 levels but CO_2/H_2O and SO_2/OCS are closer to normal passive degassing levels. Class (iv) bubbles (Table 3) also occur outside of refill periods. These also have a lower OCS/CO than class (i)–(iii) bubbles, to the extent that the smallest have almost no discernible effect on OCS, while both SO_2 and HCl levels are higher. Rock and ice collapsing into the lake can trigger small explosions [36], and such collapses are apparent in TIR images following larger explosions. However, the higher CO_2 content of small bubbles compared to passive degassing suggests a potentially deeper source.

In addition to bubbles, changes in gas ratios have been identified that do not correspond directly to 'typical' passive degassing behaviour (e.g. [29]) of the lake (Table 3). Most of these are identifiable as gentle peaks or troughs in gas ratios that occur over a longer period compared to large explosions, lasting about 10–15 min from onset to the return to typical passive degassing levels. A notable feature of these peaks (Fig. 5) is that, despite releasing higher proportions of CO_2 than during passive degassing, they are relatively rich in OCS compared to CO, in contrast to small bubbles. By considering other gas ratios we can see that, for some (but not all) such instances, proportions of CO_2, CO, and SO_2 are also affected, in that order. Corresponding changes in water, HCl, and HF, are not evident. The peaks in gas ratios are steeper before the event, with a more gradual decrease. It appears that a separate process is overprinted on the passive degassing to sustain an increased output of certain gases. Although infrequent (seven were identified), these events represent a recurrent feature of degassing.

3.3. Lake refill period

The refill of the lake after class (i) bubbles takes approximately 10 min, based on inspection of thermal images. The CO_2/CO ratios, which rapidly increase during the explosion, gradually fall to typical passive degassing signatures. For the largest explosions, it generally takes a similar time to the refill for the CO_2/CO compositions to return to previous levels. Other ratios drop below (CO_2/H_2O, CO_2/SO_2, CO_2/HCl) or rise above (SO_2/OCS) typical passive degassing values immediately after the bubbles burst, and then rise or fall back to pre-explosion levels over the next tens of seconds (see Figs 2 and 3 for examples). Oscillations are visible in gas ratios such as CO_2/CO and CO_2/SO_2 on short (approx. 5–10 s) time scales during the onset of lake recharge (Supplementary Materials). Following smaller class (iii) bubble bursts, the gas ratios return rapidly to pre-explosion levels without this perturbation.

The refill period can be difficult to study, as the gas and tephra released by the explosion typically obscures the lava lake in TIR images. The gas generally appears to have higher abundances of SO_2, water, and HCl than passive degassing. The most clearly observed refills, at 18:44 on 13 December and 16:38 on 14 December 2013, show, in addition to the pool at the lake bottom where the top of the conduit is expected [10], a second source of lava into the lake (Fig. 6). We interpret this as spattered lava draining from the crater, channelled through an area where the crater
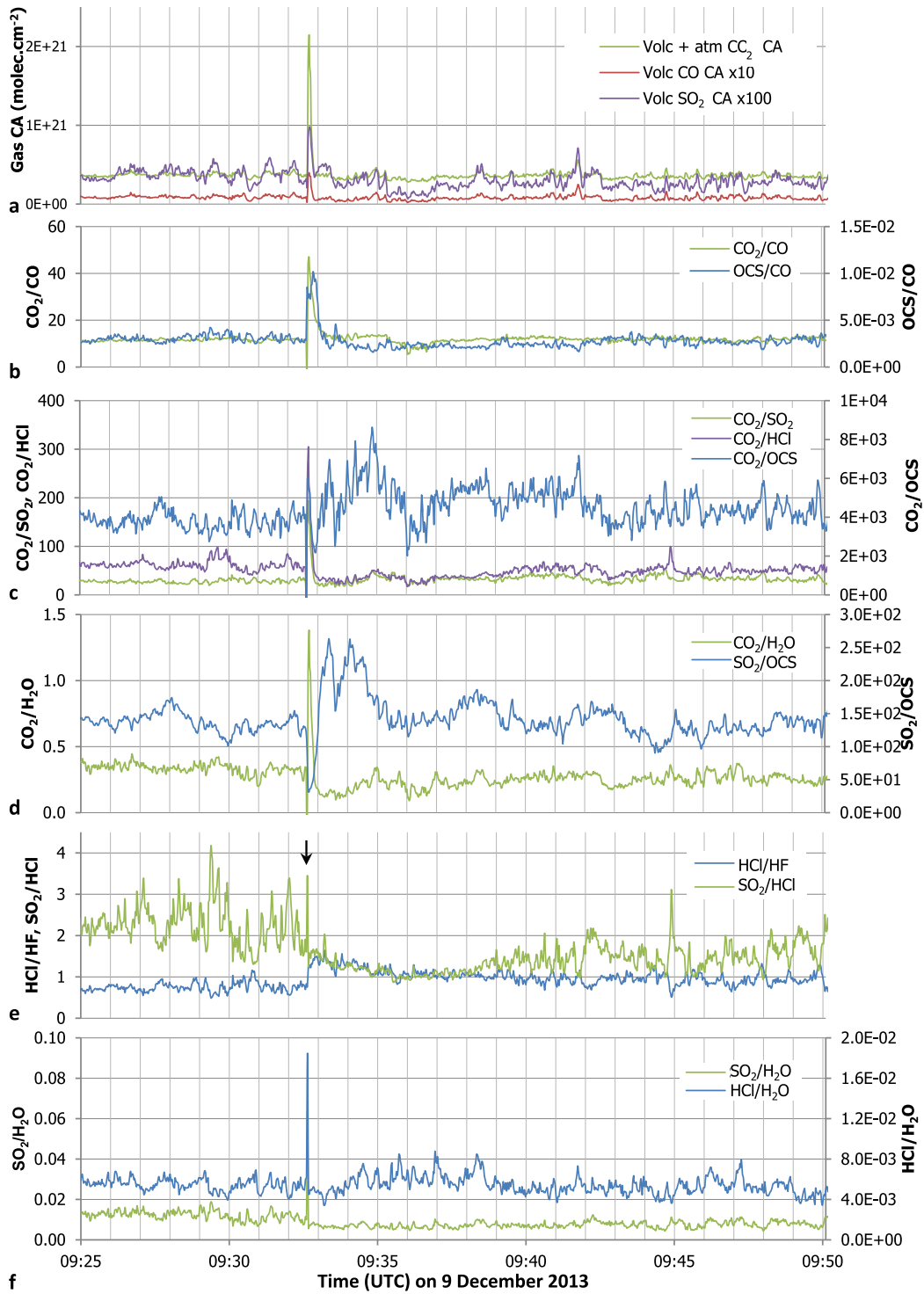
Fig. 2. Time series plots of gas ratios and column amounts (CAs) over 25 min on 9 December 2013 (UTC, vertical gridlines spaced at 1 min) spanning a class (ii) explosion shortly before 09:33. The CA for CO_2 in (a) is uncorrected for atmospheric amounts, but ratio plots (b–f) include corrections for background amounts of both CO_2 and H_2O. The corrections do not account for reduced background CO_2 and H_2O after the explosion due to shortened atmospheric pathlength, but the trends shown by the time series were verified, and gas ratios obtained, using scatter plots (Fig. 3). Note generally the peaks in CO_2/CO, CO_2/SO_2, CO_2/HCl, CO_2/H_2O and dip in SO_2/OCS coincident with the bubble burst (09:32), followed by increases in water and SO_2 above passive degassing levels relative to less soluble gases; (a) CAs peak sharply as the bubble gas is detected, and drop rapidly afterwards; (b) CO_2/CO levels recover before OCS/CO, both returning to former levels within approx. 1 min; (c) CO_2/OCS is highly variable after explosion and oscillates on periods of 2–3 min during refill while CO_2/HCl and CO_2/SO_2 spike during explosion, drop below passive levels, then recover over approx. 7 and 2 min respectively, with a hint of the same oscillation; (d) SO_2/OCS drops sharply with the explosion, increases well beyond previous levels, then recovers with faint 2–3 min cycles, while CO_2/H_2O increases rapidly, then drops below passive degassing levels and takes longer to recover; (e) The increase in both ratios due to explosion is rapid and short-lived (see black arrow) and variability is reduced for approx 10 min after explosion, with SO_2/HCl remaining below previous levels for most of this time; (f) The change in SO_2/H_2O is similar to the SO_2/HCl time series, whereas HCl/H_2O recovers very rapidly.
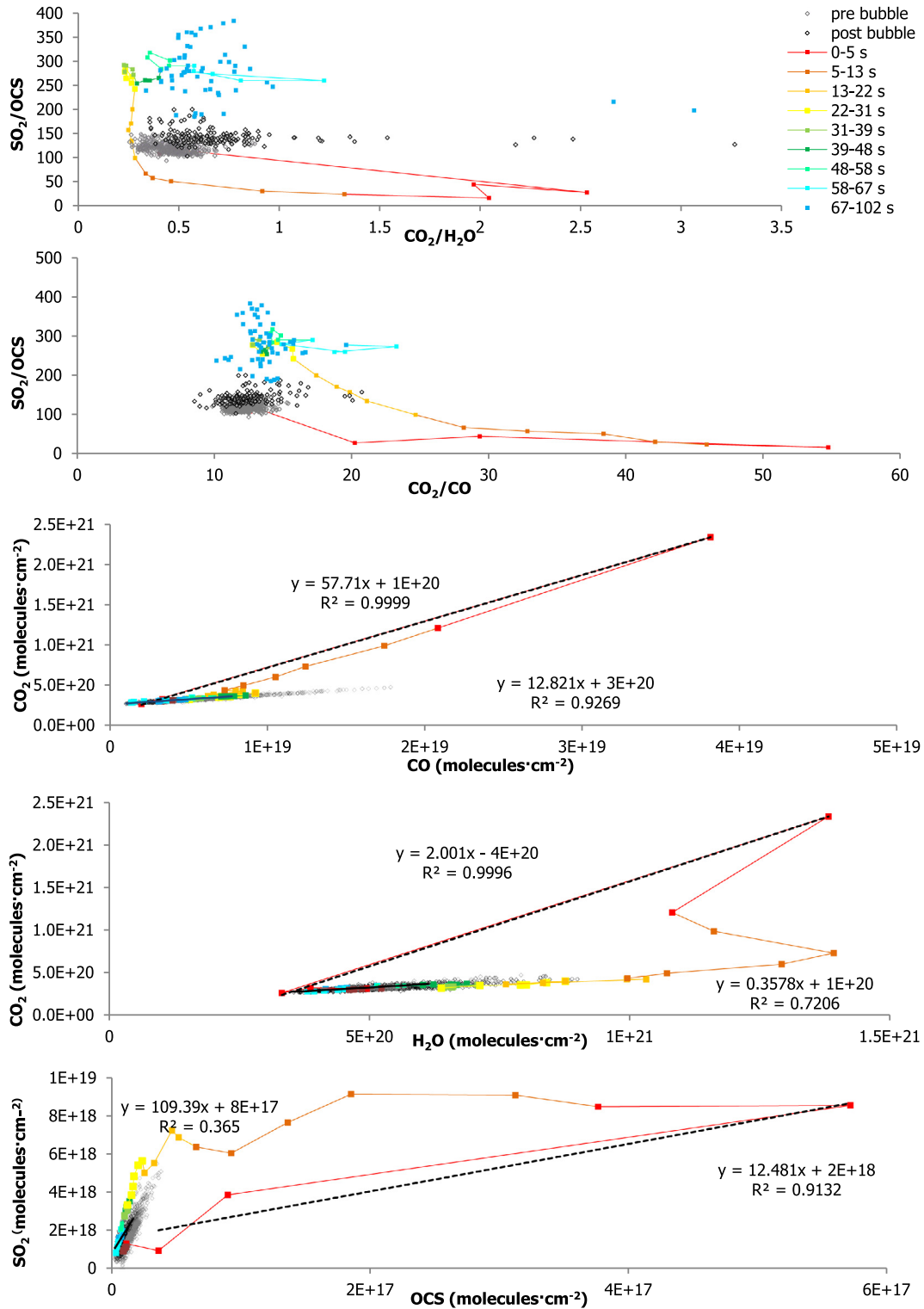
Fig. 3. Evolution of gas ratios, and of CAs of gas pairs, showing change in plume compositions before, during, and after the class (i) explosion at 19:00 on 4 December 2013. There is an initial increase in CO_2 and OCS, and a subsequent increase in water and SO_2 compared to passive degassing levels. See top right for legend. Linear fits calculated over first 0–2 s of explosion (black dashed line) and 80–172 s after explosion (black solid line).

wall is particularly steep. An alternative explanation is from observations by Dibble et al. [10] in 1987 that, sometimes after explosions, lava was visible arriving from a vent on the wall. He noted that, in two cases, the lake continued draining after the explosion, before filling from the higher vent.

4. Discussion

We first discuss the compositions of degassing events (Section 4.1), followed by the potential mechanisms responsible for the range of observed bubble sizes and gas compositions

Table 2
Molar gas ratios and calculated equilibrium temperatures (T_{eqm}) for bubble bursts in this study, in order of increasing T_{eqm}. See Supplementary Materials for images of bubbles.

Class	Date[§] & time (UTC)	CO_2/CO	SO_2/HCl	OCS/CO	CO_2/H_2O	CO_2/SO_2	SO_2/OCS	CO_2/HCl	T_{eqm} (°C)	ΔNNO[1]
i	12/12/13 07:00	69.2	1.45	0.105	1.64	185	3.22	182	771	−0.99
i	04/12/13 19:00	57.8	1.19	0.0153	2.00	216	12.5	292	836	−0.89
i	14/12/13 16:38	60.9	1.37	0.0129	2.96	254	17.1	352	844	−0.81
i	06/12/13 12:54	44.7	0.934	0.0139	1.58	84.7	9.29	139	848	−1.1
i	10/12/13 23:15	54.7	1.59	0.0152	2.44	219	14.3	387	848	−0.89
i	12/12/13 14:04	45.2	1.46	0.0717	1.12	112	11.1	175	849	−1.1
i	14/12/13 12:07	46.1	1.16	0.00983	1.93	371	10.9	447	854	−1.0
i	07/12/13 04:30	42.8	1.18	0.0184	0.632	148	15.7	175	856	−1.1
i	05/12/13 23:36	54.3	1.40	0. 00937	1.35	206	24.7	296	861	−0.85
ii	09/12/13 16:15	41.7	1.32	0.0184	0.827	134	15.4	182	864	−1.1
ii	04/12/13 06:54	52.7	1.22	0.00643	1.71	327	23.3	362	865	−0.86
ii	13/12/13 18:44	46.2	0.626	0.00577	0.659	260	29.9	163	871	−0.96
i	15/12/13 03:36	49.4	1.03	0.00988	0.964	144	31.5	149	873	−0.89
i	13/12/13 04:53	46.5	1.21	0.0246	0.912	40.8	28.7	59.2	876	−0.93
ii	09/12/13 09:33	48.3	1.27	0.00739	1.27	260	27.7	288	877	−0.90
i	11/12/13 15:02	40.7	1.06	0.0156	0.804	73.8	26.3	72.6	883	−1.0
ii	12/12/13 04:44	33.2	0.760	0.00926	0.317	140	27.0	90.5	885	−1.2
iii	07/12/13 02:43	44.7	0.501	0.00121	0.242	112	82.2	64.1	887	−0.93
ii	05/12/13 11:50	38.6	1.11	0.00898	0.736	139	29.5	157	896	−1.0
ii	11/12/13 09:41	36.5	1.28	0.0147	0.850	84.7	25.1	119	897	−1.1
ii	06/12/13 19:11	40.6	1.30	0.00922	1.13	126	33.6	166	902	−0.96
ii	13/12/13 10:00	37.6	0.910	0.00868	1.17	202	26.7	184	902	−1.0
i	14/12/13 00:26*	44.5	1.21	0.00686	0.570	89.2	64.4	106	902	−0.88
iii	10/12/13 05:00	37.1	0.704	0.00232	0.859	329	48.7	190	921	−0.98
iii	14/12/13 09:06	102	0.346	NA	0.181	128	NA	44.1	NA	NA

* Noisy spectra.
§ Format: dd/mm/yy.
[1] Calculated using CO_2/CO and T_{eqm} from D-Compress.

Table 3
Molar ratios and calculated equilibrium temperatures for selected passive degassing including preceding class (i)–(iii) explosions and during subsequent refill; small bubble bursts; and atypical degassing compositions. Full table of pre-explosion and refill compositions available in Supplementary Materials.

| Event	Date & time (UTC)	CO_2/CO	OCS/CO	CO_2/H_2O	CO_2/SO_2	SO_2/OCS	CO_2/HCl	T_{eqm} (°C)	ΔNNO
Passive[#]	02/12/13	11.8	0.00187	0.311	43.2	110	42.7	1081	−1.5
(iv) Slow event[§]	02/12/13 01:37	16.5	0.00866	0.648	58.5	17.7	108	971	−1.5
Passive	02/12/13	11.8	0.00173	0.303	48.0	127	42.4	1087	−1.5
(iv) Slow event	02/12/13 06:33	14.6	0.00281	0.534	45.8	111	55.4	1069	−1.4
Passive pre-(ii)[§]	04/12/13 06:54	12.3	0.00228	0.463	39.3	137	47.3	1101	−1.4
Refill post-(ii)	04/12/13 06:54	14.1	0.00117	0.181	18.4	448	26.7	1104	−1.3
Passive pre-(i)	04/12/13 19:00	13.1	0.00211	0.335	39.2	137	41.8	1079	−1.4
Refill post-(i)	04/12/13 19:00	19.6	0.00272	0.310	29.9	218	38.4	1039	−1.2
Passive pre-(i)	05/12/13 23:36	12.1	0.00195	0.322	37.1	155	44.2	1096	−1.5
Refill post-(i)	05/12/13 23:36	15.6	0.00221	0.265	33.1	236	43.1	1071	−1.3
(iv) Slow event	06/12/13 04:12	15.9	0.00797	0.612	42.6	34.7	72.0	1005	−1.5
Passive pre-(i)	06/12/13 12:54	12.5	0.00248	0.416	35.4	125	47.6	1089	−1.5
Refill post-(i)	06/12/13 12:54	15.7	0.00915	0.673	43.3	26.0	74.4	996	−1.5
(iv) Slow event	06/12/13 15:21	14.9	0.00376	0.552	56.2	59.8	60.4	1036	−1.4
Passive pre-(iii)	07/12/13 02:43	12.9	0.00234	0.325	25.2	162	40.3	1089	−1.4
'Refill' post-(iii)	07/12/13 02:43	11.8	0.00105	0.166	21.0	1274	22.6	1188	−1.3
Passive pre-(i)	07/12/13 04:30	12.2	0.00205	0.310	34.9	141	39.8	1088	−1.5
Refill post-(i)	07/12/13 04:30	16.8	0.00318	0.171	17.6	212	35.6	1037	−1.3
(iv) Bubble	07/12/13 04:38	20.1	0.000497	0.334	150	235	60.7	1043	−1.2
(iv) Bubble*	09/12/13 07:46	38.0	0.000469	0.427	55.6	468	172	996	−0.73
(iv) Slow event	09/12/13 09:12	14.7	0.00749	0.534	40.7	39.6	150	1018	−1.5
Passive pre-(ii)	09/12/13 09:33	12.6	0.00249	0.255	22.9	136	42.4	1074	−1.5
Refill post-(ii)	09/12/13 09:33	15.1	0.00153	0.145	22.7	279	35.9	1060	−1.4
(iv) Slow event	09/12/13 12:22	21.6	0.00586	0.751	105	27.1	147	960	−1.3
Passive pre-(iii)	10/12/13 05:00	11.4	0.00213	0.360	39.2	114	47.8	1094	−1.5
'Refill' post-(iii)	10/12/13 05:00	13.3	0.00126	0.446	25.6	380	29.0	1142	−1.3
(iv) Bubble*	10/12/13 15:02	29.6	0.000748	0.537	225	229	110	1004	−0.93
(iv) Slow event	10/12/13 16:16	12.2	0.00229	0.484	41.5	114	47.0	1094	−1.5
Passive pre-(i)	10/12/13 23:15	11.4	0.00192	0.324	41.3	138	43.4	1100	−1.5
Refill post-(i)	10/12/13 23:15	13.1	0.00140	0.169	40.0	220	45.7	1076	−1.4
(iv) Bubble	11/12/13 02:51	18.5	0.00129	0.320	57.9	247	48.8	1056	−1.2

Shaded entries indicate slow degassing events.
\# Passive degassing signatures calculated by linear regressions, with pre-bubble compositions based on the few minutes leading up to an explosion and other passive compositions calculated over tens of minutes.
§ Numerals indicate explosion class (see Section 3, Results, for explanation).
* Denotes bubbles detected seismically.
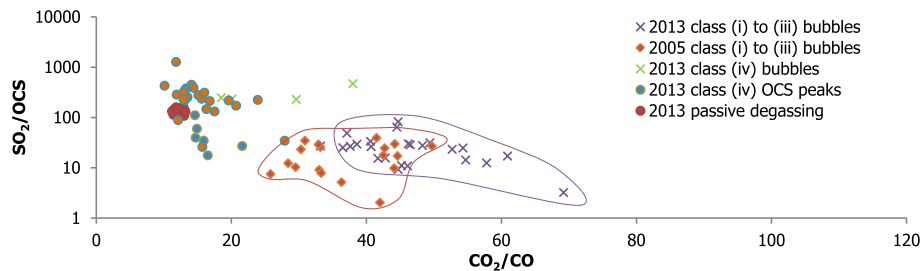
Fig. 4. Gas ratios for explosions in 2005 and 2013, and during different types of degassing in 2013 – SO_2/OCS and CO_2/CO are shown as these ratios vary most consistently. See Table 2 and SM for other ratios. Passive degassing compositions are tightly clustered; there is some overlap between compositions for 2005 and 2013 explosions. See Section 3.2 for small bubbles and OCS peaks, and Section 3.3 for refill. Note log scale on y-axis.
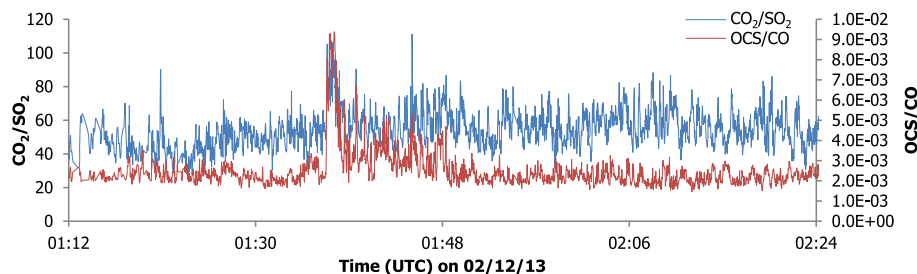
Fig. 5. Degassing anomaly at 01:33–01:48 on 02 December 2013, not accompanied by bubble bursts. Note sharp peak at onset and gradual decrease particularly evident in OCS/CO. The composition of the peak at 01:37 is given in Table 3.

(Section 4.2). We consider the implications of our observations regarding the refill period after explosions (Section 4.3). Finally (Section 4.4), we suggest a model for explosive and anomalous degassing at Erebus lava lake.

4.1. Bubble compositions

The classes of degassing events identified in 2013 appear to fall broadly into two categories: high energy class (i)–(iii) explosive events with a more oxidised composition, and class (iv) non-explosive events, with a composition closer to that of passive degassing. This spectrum of degassing has similarities to that at Stromboli, particularly in the two main groups of gas compositions that are evident ("syn-explosive" and "quiescent" plumes; [1]; however, the melt composition and higher viscosity of Erebus phonolite [24] will affect the emitted compositions and types of activity.

4.1.1. Explosions

Class (i)–(iii) bubbles are invariably more CO_2-rich than the passive degassing (Fig. 4). Despite the range of bubble sizes observed, there are common elements to their compositions – in particular, the increases in CO_2, OCS, SO_2 and CO, and relative depletion in water.

We find that class (i) explosions generally have lower equilibrium temperatures, and lower SO_2/OCS, compared to class (iii) explosions. The bomb-throwing explosions contain a large volume of gas rich in CO_2, CO, OCS and SO_2, but little fresh magma, and there is likely limited interaction between gas in the bubble and the conduit magma during ascent. Peaks in more soluble species occur after the explosion, and we attribute these to degassing of the erupted magma, now exposed to atmospheric pressure, and the rapidly refilling lake.

Subsequent smaller peaks in CO_2/CO after explosions suggest that bubbles may arrive in groups. The peaks are sharp and occur after the ratio has approached passive degassing levels. Although Gerst [12] found secondary peaks in lake surface acceleration after

some bubbles, which could be associated with a second bubble, these occurred on a much faster time scale (separated by 0.3 s) and would not be distinguishable in FTIR spectra or TIR images. Where a second explosion is detected in gas ratios, its composition is often within the passive degassing range on a scatter plot, with insufficient points to calculate a linear regression. Assuming that they are not due to crater wall collapse into the lake triggered by the explosion, or the impact of bombs, three factors are identified that may promote subsequent bubbles: the break-up of the original gas slug on ascent; increased accumulation of gas at a static point (e.g. an asperity in the conduit) that favours bubble formation; and accumulations of gas in the incoming recharge magma from the conduit. If peaks after an explosion are due to a slug breaking up, there must be a significant difference in the relative ascent rates to cause intervals of 1–2 min between the two, presumably because of the much smaller size of the trailing bubbles. Alternatively, small bubbles could be created and travel from their source in succession through the conduit magma (i.e. physically decoupled from the melt); or the magma that rises and refills the lake after the initial explosion may contain small gas bubbles (physically coupled to the melt), possibly even generating them as it vesiculates with rapid ascent and depressurisation.

Small (e.g. class (iii) and some class (iv)) explosions may have a similar source to the class (i) and (ii) explosions, but the proportion of gas emitted from the bubble compared to that exsolved from the lake magma, some of which has been disrupted and exposed to atmospheric pressures, will be lower. During ascent, gas in small bubbles is likely to re-equilibrate with the magma to a greater extent than in larger bubbles, since small bubbles have slower ascent rates and higher surface area to volume ratios. As a result, when class (iii) and (iv) bubbles explode, low pressure degassing from the lake and/or magma recharging the lake after an explosion, will release water, SO_2 and HCl in relatively high quantities; however, emission of the CO_2-rich 'bubble gas' will be less than that observed for class (i) and (ii) events. The small gas volume emitted by the explosion, relative to the degassing from the lake, will mean that measured compositions, and thus the calculated equilibrium
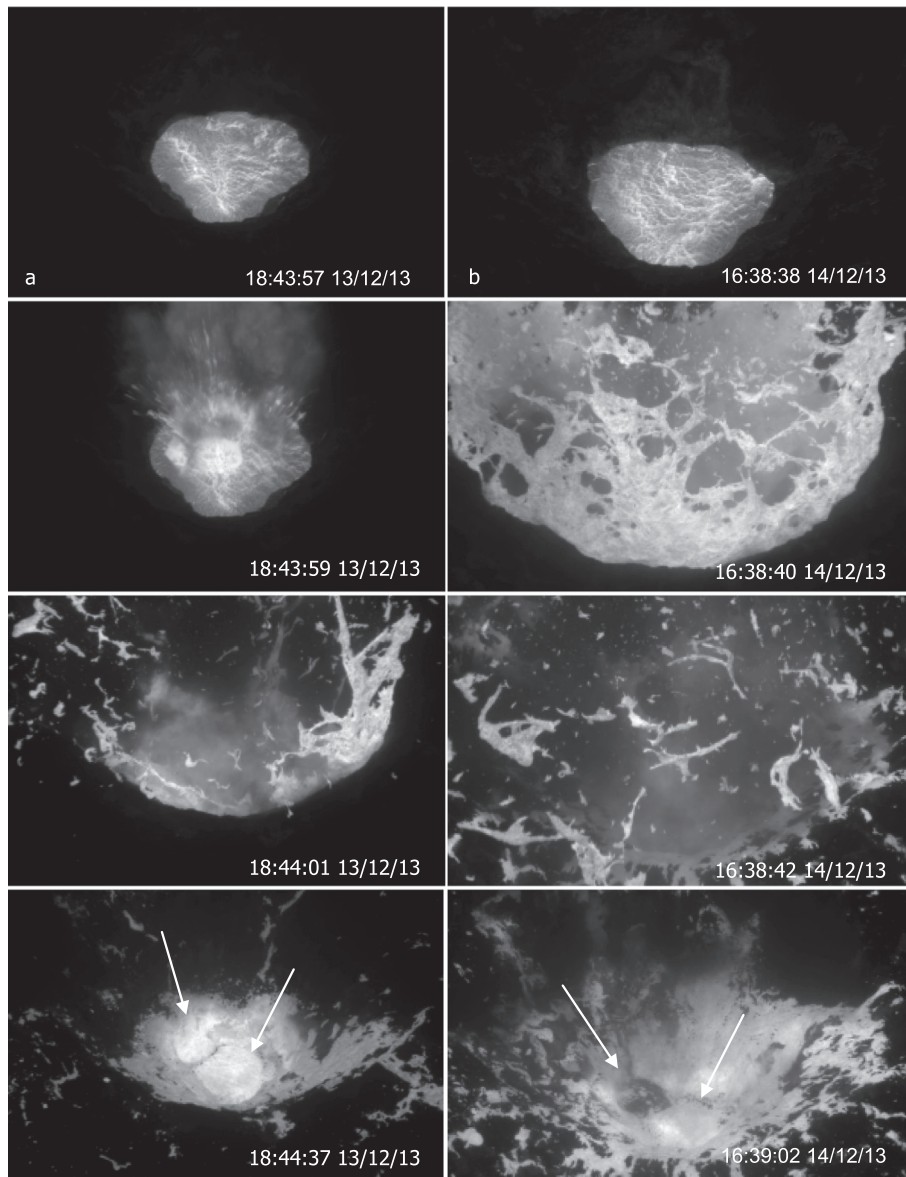
Fig. 6. Refilling of the lava lake after explosions at (a) 13/12/13 18:44 and (b) 14/12/13 16:38. Images from before and during the explosion are shown for comparison. On refill images, arrows on right show reduced lake, and arrows on left show where magma re-enters the lake, possibly from spatter that drains down the crater wall.

temperatures, may not accurately reflect the gas from the bubble but rather a mixture of passive and explosive degassing. However, amongst the large (lake-sized) bubbles, which emit more gas, the largest bubbles still have lower equilibrium temperatures compared to smaller bubbles.

Calculations by Burton et al. [7] for degassing at Stromboli show that explosion gases have much higher equilibrium temperatures than passive degassing, suggesting that their compositions more closely reflect their source conditions. The cooler temperatures for Erebus explosions may be due to adiabatic bubble expansion. Table 2 includes equilibrium temperatures calculated by D-Compress at atmospheric pressure (610 hPa) for gases released from bubbles. We expect the largest bubbles to have a higher degree of cooling or overpressure, and Burgisser et al. [6] showed that shallow adiabatic expansion and cooling can account for the observed equilibrium temperatures of explosion gas (see Supplementary Materials). We note, however, that equilibrium temperature calculations have high associated uncertainty. In addition to increased fitting errors for explosion spectra

(Section 2.3), there are uncertainties in the parameters used for retrieving gas ratios, so it is plausible that explosive gas temperatures are more similar to one another than equilibrium calculations indicate. Here, we estimate an uncertainty of 20%, from the discrepancy of up to 15% between T_{eqm} calculated here and by Burgisser et al. [6], combined with 5% uncertainty in D-Compress [6].

Despite changes to the morphology of the Inner Crater over this time (for instance, the surface area of the lake in 2013 was at about half that in 2005; [22], the explosion styles appear to be consistent between episodes of increased activity. There are a few potential reasons for the increased frequency of explosions in 2005 and 2013, and in previous years such as 1984–88. The accumulation of gas to form large bubbles could be promoted by asperities in the conduit [26]. Another possibility is that properties of the magma – increased viscosity, for example, or increased gas supply due to recharge of a deeper magma chamber – favour more frequent accumulation of gas. However, the geochemistry of bombs and lava flows have remained very consistent over time [23],

which indicates that changes to temperature and viscosity are unlikely. Although Caldwell and Kyle [8] propose that a phonolite injection into the magma chamber could have provided the volatiles to trigger the episode in 1984, more recent studies of SO_2 flux do not show any marked differences during 2005 [37]. This suggests that the latest explosive episodes, at least, are not driven by changes to melt chemistry or gas supply. This leaves the variation of conduit geometry as the most likely cause for changes in explosion frequency.

4.1.2. Non-explosive events (class (iv))

Class (iv) bubbles are different in composition; for example, CO_2/H_2O is slightly lower, and the higher water content compared to class (i)–(iii) bubbles may indicate more shallow degassing relative to the larger bubbles. Peters et al. [34] found no correlation between the phase in passive degassing cycles and the timing of class (iv) bubbles, and of the four class (iv) bubbles identified here for which changes in degassing could be measured, two were detected seismically and have slightly higher CO_2/CO and CO_2/H_2O ratios. These findings could reflect multiple processes creating small bubbles, which would also account for the observed range of CO_2/CO ratios.

At the low energy end of the degassing spectrum are discrete degassing events that occur over minutes. The gas released may have a similar, H_2O-depleted signature to large bubbles, but preserves less of its source composition and is less affected by expansion (e.g. having a lower CO_2/CO ratio). Instead of the increase in water and HCl that is typical at the peak of passive degassing cycles, there is a greater increase in OCS, CO_2, and CO (and, to a lesser extent, SO_2). These events, when apparent in FTIR retrievals, last several minutes and involve higher levels of CO_2 and OCS degassing compared to the background, while CO_2/H_2O remains within the range for passive degassing. A decrease in this ratio might suggest increased shallow degassing in the lake, whereas here, it is more likely that the gas content of incoming magma has increased, perhaps due to the same processes (e.g. increased gas supply) responsible for creating bubbles. A comparison with mean and maximum lake velocity shows no notable difference during these events, nor is there an obvious relationship between these perturbations and bubble bursts.

4.2. Gas segregation

The range of bubble sizes observed at Erebus include those producing explosions and those small enough to be considered normal passive degassing behaviour. However, it is possible that all of these bubbles are generated by the same mechanisms but vary in size, ascent rate, and overpressure. In this section, we consider how the observed gas compositions might reflect the bubble origins and ascent conditions.

Explosions at Erebus are usually described as Strombolian activity [5]. Models for Strombolian eruptions in low viscosity magmas are generally divided into two types: those driven by gas accumulation as a foam, and its subsequent collapse into 'gas pockets' (e.g. [19,18]) and those related to the relative ascent rates of bubbles and magma (e.g. [32]). Both models include Strombolian and Hawaiian eruptions as two end-members, but the mechanisms they invoke for Strombolian eruptions are not mutually exclusive. We next consider how the depths of accumulation and the extent of coupling between gas and melt relate to transient degassing compositions at Erebus.

The compositions of the larger bubbles among the class (i)–(iii) events correspond to lower equilibrium temperatures, indicating re-equilibration in the gas phase due to adiabatic cooling [6,2]. The range in explosivity, and correspondingly in overpressure, appears related to the volume and ascent rate of the bubbles.

Higher overpressures are likely to be associated with rapid ascent and/or higher gas volumes. In accordance with observations made by Dibble et al. [10], large explosions can result from faster, elongated slugs producing jet-like eruptions with smaller pyroclasts, as well as slower bubbles that appear more spherical and produce only larger bombs. The infrared images, at present frame rates, cannot give any further indication of the shapes of the bubbles and their explosions, but the gas compositions of both types are similar. Furthermore, based on the data studied here, compositions of all explosive bubbles large enough to be measured by FTIR spectroscopy, i.e. class (i) to (iii) do not appear significantly different.

Class (iv) bubbles, which are different in composition, could be formed either at shallow depths, similar to the gases released during passive degassing, or at greater depths but have more interaction with the melt. This would account for their smaller size and lower CO_2/H_2O ratios compared to explosive bubbles, despite the wide range of CO_2/CO ratios observed. Class (iv) slow degassing events may represent accumulated gases that did not acquire enough volume to decouple, and that have continued re-equilibrating with the melt during ascent. Alternatively, they could be gases that have decoupled without sufficient overpressure to break through the cooled lava lake crust, and instead are released through cracks over a longer period.

Burgisser et al. [6] found that gas rise from a source at a maximum of a few hundred bars could account for measured explosion compositions in 2005–06. They also showed that CO_2/H_2O ratio is not influenced strongly by adiabatic expansion, and inferred that slug rise is initially slow, allowing the addition of volatiles from the surrounding melt, followed by acceleration of the slug. The higher CO_2/H_2O ratios of the class (i) and (ii) bubbles could therefore be explained by their decoupling from the melt at greater depth, whereas smaller class (iii), and some class (iv), bubbles continue to re-equilibrate with the surrounding melt. The initial CO_2/CO ratios may also be similar, but for larger bubbles this would be increased by adiabatic cooling, whereas for smaller bubbles it might be affected by equilibration with the melt. Thus the populations observed in scatter plots would represent two end-members: gases that have segregated sufficiently at depth to decouple from the melt and form an explosive overpressured bubble, and passive degassing from the shallow melt. Class (iv) events appear to fall between the two end-members of this spectrum, but this may reflect their smaller volume and dilution by passive degassing in FTIR measurements, rather than their origins.

A similar spectrum of activity has been observed at other open vent volcanoes; for example, at Stromboli, James et al. [17] described a range from passive bubble bursts to Strombolian explosions. On the high energy end of the spectrum, slug formation and re-equilibration depths may vary significantly between volcanoes. Large gas slugs at Stromboli may decouple from the melt at much greater depths (up to 2.7 km; [7]) than expected at Erebus. Gas slugs have also been observed at lava lakes such as Kīlauea, where depths of accumulation could be up to 900 m [11] and pistoning activity may even be driven by gas accumulation beneath a crust on the lava lake [20]. However, these magmas are of lower viscosity than Erebus [24], the slug overpressures are lower, and gas release is slower.

The smaller scale events are less comparable between sites, particularly as they may be generated by multiple mechanisms. Gas puffing from smaller bubbles is a persistent form of degassing at Stromboli, in addition to passive degassing [15,35]. However, it is not clear whether class (iv) bubbles at Erebus could be similar to those causing puffing at Stromboli and, with limitations on accurate measurements of their compositions, we cannot identify distinct class (iv) bubble types generated by different processes (e.g. rockfall or gas accumulation and rise from depth). The gas pistoning mechanism described by Orr and Rea [31] at Puʻu ʻŌʻō, on

longer timescales up to tens of minutes, relates to shallow gas accumulation leading to the formation of a lava crust, and rapid gas escape. While gas release on this scale is not observed at Erebus except during explosive eruptions, shallow accumulation of smaller gas volumes beneath a viscous crust could also be responsible for the slow degassing events at Erebus.

4.3. Lake refill period

We assume that the rapid refill of the lake is due to the disruption of bidirectional equilibrium flow, as magma in the conduit reverts temporarily to a mostly unidirectional flow to restore the lake level dictated by overpressure in the magma reservoir. The source of the gas emitted during refill and, in particular, whether it is fresh magma or recycled magma from the lake, depends on the dynamics of the bubble explosion. It is unlikely that the explosion pushes lake magma back down the conduit [9,13] but magma from the lake will drain around the bubble as it ascends [39]. The volumetric flow rate during recharge was calculated, for a small class (ii) 2010 eruption, by Jones et al. [22] as >6 $m^3 s^{-1}$. For a conduit of 5 m diameter, extending 500 m to a shallow magma body [41], this rate suggests that magma recharge from the chamber would take tens of minutes to reach the lake. Thus the immediate sources of recharge are the magma already in the shallow conduit and the increased gas volume fraction from this magma due to unloading, although this response to depressurisation could propagate down the conduit to the magma storage region (e.g. [4]. The potential for other pathways by which gas or magma enter the lake further complicates the interpretation of refill gas compositions.

The change in gas ratios during the refill (Fig. 4) could result from increased magmatic degassing at shallow levels, but also a decrease in emission of more deeply-sourced gas through the permeable conduit [16] following the explosion. The CAs of CO_2 and CO during refill never appear to drop below the passive degassing range, suggesting that their supply from depth is maintained through the refill period. Despite this, there is a drop below the passive degassing range in CO_2/H_2O, CO_2/SO_2 and CO_2/HCl ratios during refill is consistent with an influx of fresh magma producing increased amounts of water, SO_2, and HCl. In smaller class (iii) events, the return to passive degassing does not show this deviation, probably because there is not a significant influx of magma following the bubble(s). Instead, SO_2 and H_2O abundances stay within normal passive degassing bounds, while OCS and CO_2 drop gradually to passive degassing levels. The small scale oscillations at the start of the refill could be due to changing proportions of refill and explosion gas, but we note that they have a similar frequency to oscillations found in VLP spectra by Aster et al. [4], who attributed them to the surging recharge of the lava lake.

Gases emitted during the refill (Table 3) typically have higher CO_2/CO and lower CO_2/H_2O than during passive degassing prior to the explosion. One explanation is that bidirectional flow in the conduit provides a continuous background 'conduit' gas flow from depth (e.g. [29]), containing a greater proportion of CO and CO_2, as well as an intermittent H_2O- and SO_2- rich 'lake' gas sourced at shallow depths from incoming magma batches. Both of these are interrupted by the explosion; then, during the refill period, degassing is dominated by H_2O-rich gas exsolved from shallow magma. An increase in deeply sourced 'conduit'-type gases (that have higher CO and lower H_2O content) occurs later in the refill, and this could be due to a number of reasons. The first is that, based on the bidirectional flow model, magma initially refilling the lake includes magma that had degassed in the lake and started to return down the conduit before the explosion. This magma will already have low gas content, and it takes some time for more deeply sourced gases to reach the surface. Another explanation is that shallow (but not recycled) magma is available for refill, but that there is a

delay in the arrival of 'conduit' gas to the passively degassing system, compared to the time taken for the lake to recharge from this shallow source. Thirdly, the bubble may have been formed by an accumulation of 'conduit' gas at an asperity, temporarily depleting the supply. Finally, since some component of the gas measured after an explosion remains within the crater for seconds to minutes, the composition of the gas emitted during refill cannot be wholly isolated. The fourth possibility, therefore, is that the FTIR measurements are dominated by explosion gas, and changes to the conduit degassing are minimal by comparison until the explosion gas disperses. Spattered lava continues degassing during this time and, as it drains back into the crater, may also have an effect on the gas composition measured by the spectrometer. The lower equilibrium temperatures for refill compositions after class (i) explosions (Table 3) are consistent with such degassing of cooled and recycled lava from the eruption; however, these temperature calculations may be influenced by CO_2-rich gas from the explosion remaining within the crater.

4.4. Synthesis

4.4.1. Explosive events – class (i)–(iii)

Explosions at Erebus share similarities in gas composition that set them apart from small bubble bursts, other transient degassing events, and passive degassing. We suggest that explosions occur as a result of increased gas input to the lava lake (Fig. 7a–c). The gases in explosive bubbles are sourced from more oxidised conditions to those emitted during passive degassing, and there is disequilibrium between the gas and the magma through which it erupts; i.e. it has last equilibrated with the magma under deeper and more oxidised conditions [27]. The monitored gas composition changes instantaneously with large explosions, reflecting the higher content of CO_2 in the associated bubbles, and the rate at which the volume of gas previously in the bubble occupies and dominates the optical path between the crater rim and the lava lake. The variation in gas compositions emitted by explosive bubbles may be due to different ascent rates and the degree of adiabatic expansion.

There is an overlap in explosion compositions and equilibrium temperatures between periods of greater activity in 2005–06 and 2013, suggesting that processes driving large explosions have not changed significantly. The difference in gas ratios, particularly the higher CO_2/CO in 2013, may be due to a lower depth of sequestration (in addition to retrieval and calculation uncertainties), resulting in a more oxidised source, or greater expansion and adiabatic cooling of rising bubbles. The progressive subsidence of the crater floor over several years [22] could be a surface expression of the progressive decrease in the magma column height and gas supply over time.

4.4.2. Non-explosive events – class (iv)

Non-explosive transient degassing events have a relatively reduced gas composition, closer to that of the passive degassing regime. This suggests either a different source to the explosions, or a greater degree of re-equilibration with the melt. For example, small peaks in gas emissions may be due to small (metres-scale) bubbles produced either by similar mechanisms to the explosions (Fig. 7d), or by collapses of wall rock and ice into the lake. Much smaller, dispersed, gas bubbles could account for the gradual degassing events characterised by an increase and decrease in OCS, CO_2, CO, and SO_2 emissions, over periods of seconds to minutes, with no obvious physical change in lake activity. Passive degassing would represent gas rising through a permeable conduit as well as degassing from melt within the lake; small bubbles, either gas that was partially trapped within the melt but continued to rise, re-equilibrating with the melt, or gas that exsolved at shallow depths; and larger bubbles, gas that was trapped until a
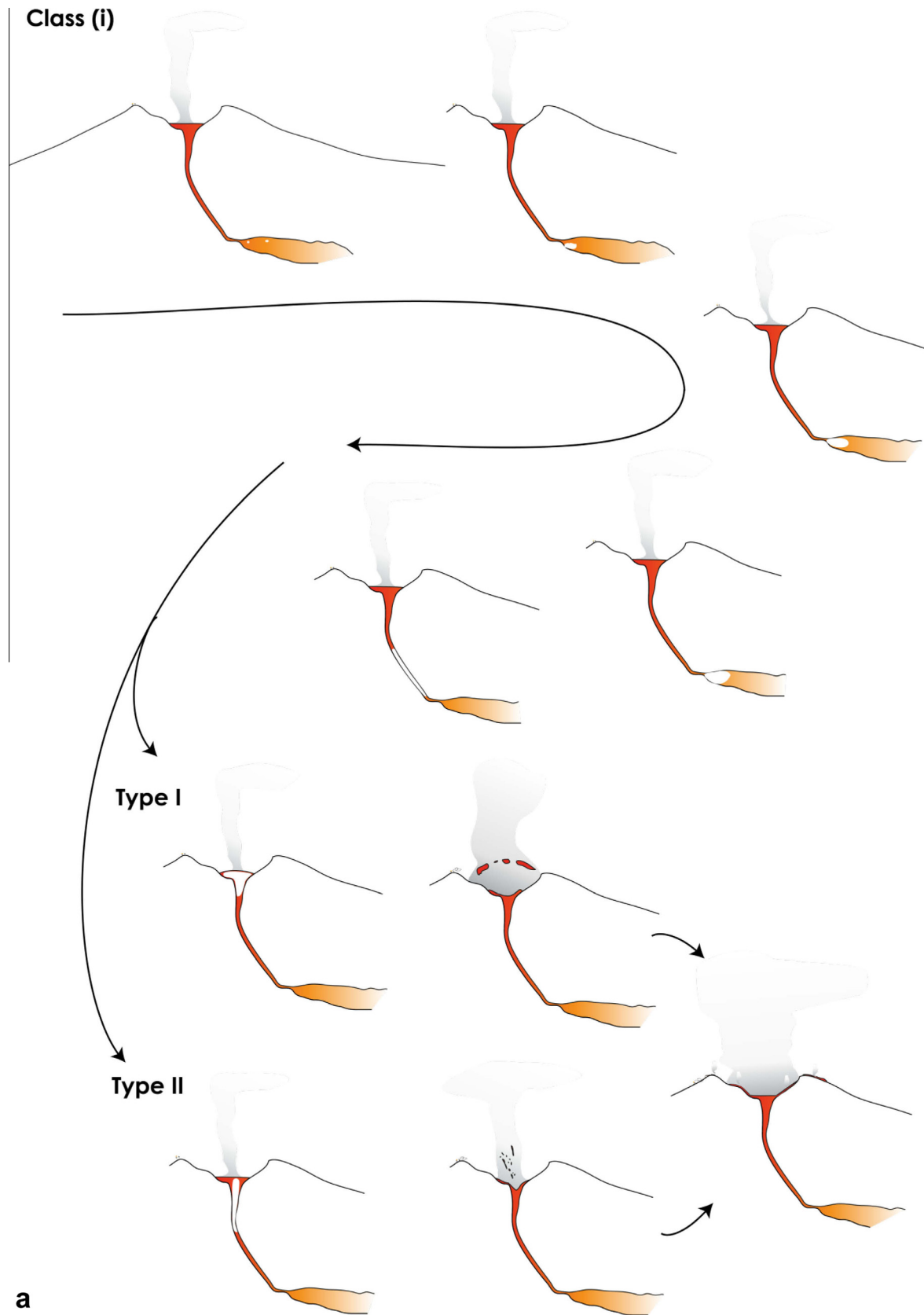
Fig. 7. Gas segregation and ascent resulting in different classes of transient degassing events (a–d represent classes (i)–(iv)). Class (i) involves largest volumes and overpressures; type divisions after Gerst [12]. Class (iii)–(iv) events have smaller volumes and slower ascent, so remain coupled to melt until shallower depths, and lower burst pressures.
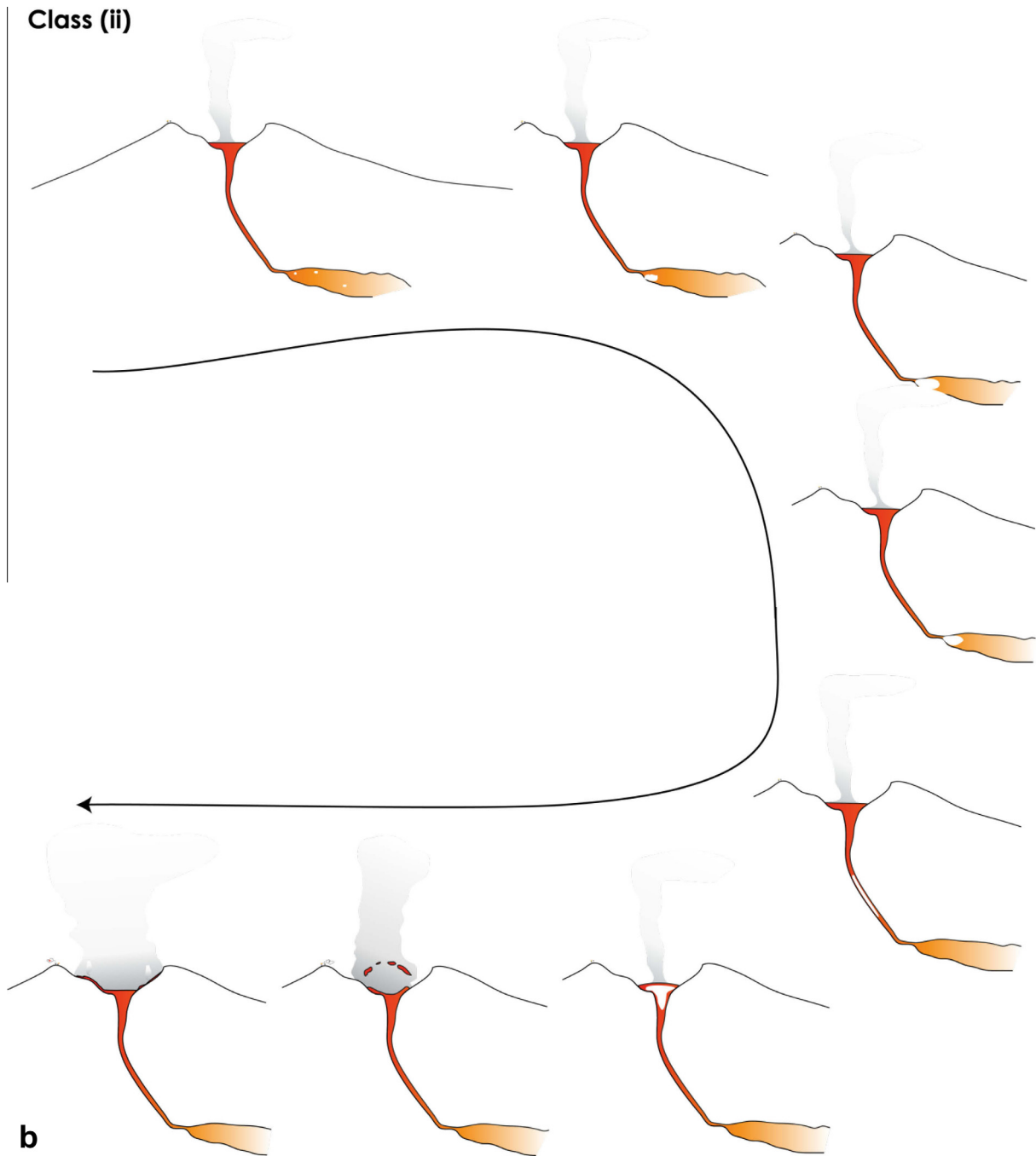
Class (ii)

Fig. 7 (*continued*)

4.4.3. Refill period

Lava ejected from the lake during explosions may cause a peak in degassing of species such as water, SO_2, or HCl. Large explosions are followed by secondary increases in SO_2, H_2O, and HCl degassing, after the dispersal of the bubble gas, as the lake is emptied during the explosion and refills. This peak also occurs in CO_2/CO and OCS/CO ratios but, despite the potential for CO_2-rich explosion gas to remain in the crater, ratios of CO_2/SO_2 and CO_2/H_2O drop even below 'normal' background levels. The disruption of bidirectional flow and influx of magma

sufficient volume was reached to form an explosive gas slug (Fig. 7).

from the conduit is partly responsible for increased water and SO_2 emission. We expect the gas emitted during refill more closely reflects the composition of shallow sourced magma, with higher water and SO_2 content, whereas the typical passive degassing of the lake, including cyclic behaviour, often contains a higher proportion of CO_2 and CO rising from greater depths. This indicates that shallow magma is available to recharge the lake when the magmastatic pressure drops [40] after it is emptied by explosions. Two likely sources of refill gas are erupted lava draining back into the lake, and descending degassed magma from the passive degassing regime. Some part of the refill composition may also be due to the slow dispersal of explosion gases remaining in the measurement path.
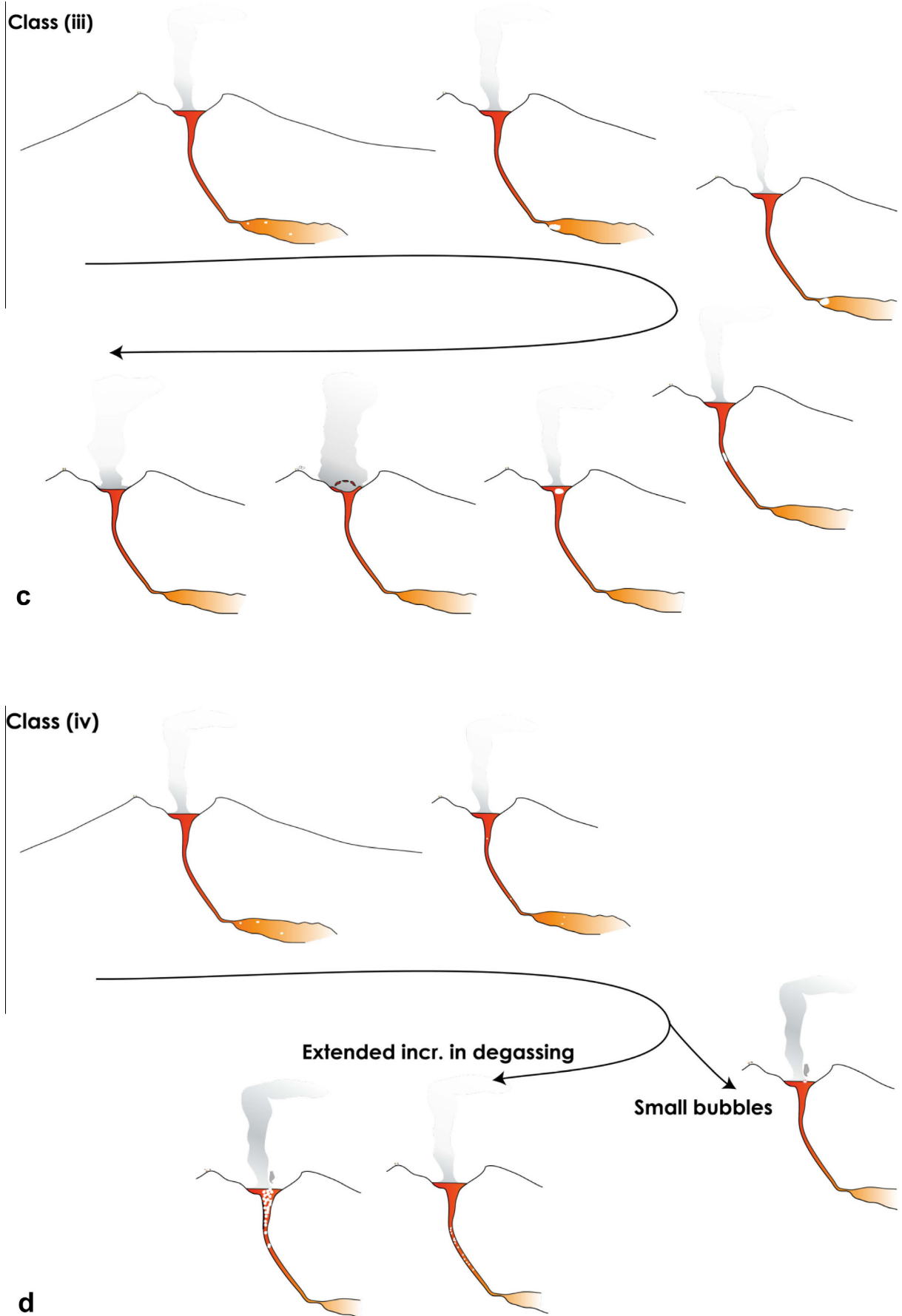
Class (iii)

c

Class (iv)

Extended incr. in degassing

Small bubbles

d

Fig. 7 (*continued*)

5. Conclusions

We find that the compositions of explosive bubbles in the latest episode of increased eruptive activity at Erebus are similar to those from 2005–06, and characterised by more oxidised compositions than passive degassing. In addition to explosive activity, two types of anomalous degassing events (small bubble bursts and longer duration increases in emissions of some gases, particularly OCS) have been identified that have more variable compositions than passive degassing and that appear to be associated with a smaller gas volume.

Both explosive and non-explosive events may result from gas segregation, with a sufficient accumulation of gas resulting in an explosion. Such bubbles preserve some evidence of the source composition (e.g. CO_2/H_2O ratios, which are similar regardless of bubble class and size) but adiabatic expansion alters some of the original gas (e.g. CO_2/CO ratios, which are roughly related to bubble size). Smaller accumulations of gas may result in other forms of anomalous degassing, including small bubbles; but similar bubbles may also be caused at shallow depths, for example by rock and ice fall into the lake.

Finally, refill compositions are more variable than passive degassing, reflecting the increased sources of gas in the crater, including remnant explosion gas; spatter, and erupted lava draining back into the lake; and magma from the conduit. The latter is likely a combination of degassed magma returning down the conduit as a result of bidirectional flow, and fresh magma recharge.

Acknowledgements

Appendix A. Supplementary data

Supplementary data associated with this article can be found, in the online version, at http://dx.doi.org/10.1016/j.grj.2015.05.001.

References

[1] Aiuppa A, Bertagnini A, Métrich N, Moretti R, Di Muro A, Liuzzo M, et al. A model of degassing for Stromboli volcano. Earth Planet Sci Lett 2010;295:195–204. http://dx.doi.org/10.1016/j.epsl.2010.03.040.

[2] Alletti M, Burgisser A, Scaillet B, Oppenheimer C. Chloride partitioning and solubility in hydrous phonolites from Erebus volcano: a contribution towards a multi-component degassing model. GeoResJ 2014;3–4:27–45. http://dx.doi.org/10.1016/j.grj.2014.09.003.

[3] Aster R, McIntosh WC, Kyle PR, Esser R, Bartel B, Dunbar NW, et al. Real-time data received from Mount Erebus volcano, Antarctica. EOS Trans Am Geophys Union 2004;85:97–104.

[4] Aster R, Zandomeneghi D, Mah S, McNamara S, Henderson DB, Knox H, et al. Moment tensor inversion of very long period seismic signals from Strombolian eruptions of Erebus volcano. J Volcanol Geotherm Res 2008;177:635–47.

[5] Blackburn EA, Wilson L, Sparks RSJ. Mechanisms and dynamics of Strombolian activity. J Geol Soc Lond 1976;132:429–40. http://dx.doi.org/10.1144/gsjgs.132.4.0429.

[6] Burgisser A, Oppenheimer C, Alletti M, Kyle PR, Scaillet B, Carroll MR. Backward tracking of gas chemistry measurements at Erebus volcano. Geochem Geophys Geosyst 2012;13. http://dx.doi.org/10.1029/2012GC004243.

[7] Burton MR, Allard P, Muré F, La Spina A. Magmatic gas composition reveals the source depth of slug-driven Strombolian explosive activity. Science 2007;317:227–30. http://dx.doi.org/10.1126/science.1141900.

[8] Caldwell DA, Kyle PR. Mineralogy and geochemistry of ejecta erupted from Mount Erebus, Antarctica, between 1972 and 1986. In: Volcanological and environmental studies of Mount Erebus. Antarctica: Antarctic Research Series, AGU; 1994. p. 147–62.

[9] Dibble RR. Velocity modeling in the erupting magma column of Mount Erebus, Antarctica. In: Volcanological and environmental studies of Mount Erebus. Antarctica: Antarctic Research Series, AGU; 1994. p. 17–33.

[10] Dibble RR, Kyle PR, Rowe CA. Video and seismic observations of Strombolian eruptions at Erebus volcano, Antarctica. J Volcanol Geotherm Res 2008;177:619–34. http://dx.doi.org/10.1016/j.jvolgeores.2008.07.020.

[11] Edmonds M, Gerlach TM. Vapor segregation and loss in basaltic melts. Geol 2007;35(8):751–4.

[12] Gerst A. The first second of a Strombolian volcanic eruption (Ph.D). University of Hamburg, Germany; 2010.

[13] Gerst A, Hort M, Aster R, Johnson JB, Kyle PR. The first second of volcanic eruptions from the Erebus volcano lava lake, Antarctica—Energies, pressures, seismology, and infrasound. J Geophys Res Solid Earth 2013;118:3318–40. http://dx.doi.org/10.1002/jgrb.50234.

[14] Gerst A, Hort M, Kyle PR, Vöge M. 4D velocity of Strombolian eruptions and man-made explosions derived from multiple Doppler radar instruments. J Volcanol Geotherm Res 2008;177:648–60. http://dx.doi.org/10.1016/j.jvolgeores.2008.05.022.

[15] Harris A, Ripepe M. Temperature and dynamics of degassing at Stromboli. J Geophys Res 2007;112:B03205.

[16] T. Ilanko, C. Oppenheimer, A. Burgisser, P.R. Kyle, Cyclic degassing of Erebus volcano, Antarctica, Bull Volcanol, forthcoming 2015, http://dx.doi.org/ 10.1007/s00445-015-0941-z.

[17] James MR, Lane SJ, Wilson L, Corder SB. Degassing at low magma-viscosity volcanoes: quantifying the transition between passive bubble-burst and Strombolian eruption. J Volcanol Geotherm Res 2009;180:81–8. http://dx.doi.org/10.1016/j.jvolgeores.2008.09.002.

[18] Jaupart C, Vergniolle S. The generation and collapse of a foam layer at the roof of a basaltic magma chamber. J Fluid Mech 1989;203:347–80. http://dx.doi.org/10.1017/S0022112089001497.

[19] Jaupart C, Vergniolle S. Laboratory models of Hawaiian and Strombolian eruptions. Nature 1988;331:58–60. http://dx.doi.org/10.1038/331058a0.

[20] Johnson JB, Harris AJ, Hoblitt RP. Thermal observations of gas pistoning at Kilauea Volcano. J Geophys Res 2005;110(B11):B11201.

[21] Jones KR, Johnson JB, Aster R, Kyle PR, McIntosh WC. Infrasonic tracking of large bubble bursts and ash venting at Erebus volcano, Antarctica. J Volcanol Geotherm Res 2008;177:661–72. http://dx.doi.org/10.1016/j.jvolgeores.2008.02.001.

[22] Jones LK, Kyle PR, Oppenheimer C, Frechette JD, Okal MH. Terrestrial laser scanning observations of geomorphic changes and varying lava lake levels at Erebus volcano, Antarctica. J Volcanol Geotherm Res 2015;295:43–54. http://dx.doi.org/10.1016/j.jvolgeores.2015.02.011.

[23] Kelly PJ, Kyle PR, Dunbar NW, Sims KWW. Geochemistry and mineralogy of the phonolite lava lake, Erebus volcano, Antarctica: 1972–2004 and comparison with older lavas. J Volcanol Geotherm Res 2008;177:589–605. http://dx.doi.org/10.1016/j.jvolgeores.2007.11.025.

[24] Le Losq C, Neuville DR, Moretti R, Kyle PR, Oppenheimer C. Rheology of phonolitic magmas – the case of the Erebus lava lake. Earth Planet Sci Lett 2015;411:53–61.

[25] Mah S. Discrimination of Strombolian eruption types using Very Long Period (VLP) seismic and video observation at Mt. Erebus, Antarctica (M.S. Independent study). New Mexico Institute of Mining and Technology, USA; 2003.

[26] Menand T, Phillips JC. Gas segregation in dykes and sills. J Volcanol Geotherm Res 2007;159:393–408. http://dx.doi.org/10.1016/j.jvolgeores.2006.08.003.

[27] Moussallam Y, Oppenheimer C, Scaillet B, Gaillard F, Kyle PR, Peters N, et al. Tracking the changing oxidation state of Erebus magmas, from mantle to surface, driven by magma ascent and degassing. Earth Planet Sci Lett 2014;393:200–9. http://dx.doi.org/10.1016/j.epsl.2014.02.055.

[28] Oppenheimer C, Kyle PR. Probing the magma plumbing of Erebus volcano, Antarctica, by open-path FTIR spectroscopy of gas emissions. J Volcanol Geotherm Res 2008;177:743–54. http://dx.doi.org/10.1016/j.jvolgeores.2007.08.022.

[29] Oppenheimer C, Lomakina AS, Kyle PR, Kingsbury NG, Boichu M. Pulsatory magma supply to a phonolite lava lake. Earth Planet Sci Lett 2009;284:392–8. http://dx.doi.org/10.1016/j.epsl.2009.04.043.

[30] Oppenheimer C, Moretti R, Kyle PR, Eschenbacher A, Lowenstern JB, Hervig RL, et al. Mantle to surface degassing of alkalic magmas at Erebus volcano, Antarctica. Earth Planet Sci Lett 2011;306:261–71. http://dx.doi.org/10.1016/j.epsl.2011.04.005.

[31] Orr TR, Rea JC. Time-lapse camera observations of gas piston activity at Pu'u 'Ō'ō, Kīlauea volcano, Hawai'i. Bull Volcanol 2012;74:2353–62. http://dx.doi.org/10.1007/s00445-012-0667-0.

[32] Parfitt EA, Wilson L. Explosive volcanic eruptions—IX. The transition between Hawaiian-style lava fountaining and Strombolian explosive activity. Geophys J Int 1995;121:226–32.

[33] Peters N, Oppenheimer C, Killingsworth DR, Frechette J. Correlation of cycles in lava lake motion and degassing at Erebus volcano, Antarctica. Geochem Geophys Geosyst 2014. doi: 10.1002/2014GC005399.

[34] Peters N, Oppenheimer C, Kyle PR, Kingsbury NG. Decadal persistence of cycles in lava lake motion at Erebus volcano, Antarctica. Earth Planet Sci Lett 2014;395:1–12. http://dx.doi.org/10.1016/j.epsl.2014.03.032.

[35] Ripepe M, Donne DD, Harris A, Marchetti E, Ulivieri G. Dynamics of Strombolian activity. In: The Stromboli volcano: an integrated study of the 2002–2003 eruption, geophysical monograph series. Washington, DC: American Geophysical Union; 2013. p. 39–48.

[36] Rowe CA, Aster R, Kyle PR, Dibble RR, Schlue JW. Seismic and acoustic observations at Mount Erebus volcano, Ross Island, Antarctica, 1994–1998. J Volcanol Geotherm Res 2000;101:105–28.

[37] Sweeney D, Kyle PR, Oppenheimer C. Sulfur dioxide emissions and degassing behavior of Erebus volcano, Antarctica. J Volcanol Geotherm Res 2008;177:725–33. http://dx.doi.org/10.1016/j.jvolgeores.2008.01.024.

[38] Tazieff H. Permanent lava lakes: observed facts and induced mechanisms. J Volcanol Geotherm Res 1994;63:3–11. http://dx.doi.org/10.1016/0377-0273(94)90015-9.

[39] Vergniolle S, Brandeis G, Mareschal J-C. Strombolian explosions: 2. Eruption dynamics determined from acoustic measurements. J Geophys Res Solid Earth 1996;101:20449–66.

[40] Witham F, Llewellin EW. Stability of lava lakes. J Volcanol Geotherm Res 2006;158:321–32. http://dx.doi.org/10.1016/j.jvolgeores.2006.07.004.

[41] Zandomeneghi D, Aster R, Kyle PR, Barclay A, Chaput J, Knox H. Internal structure of Erebus volcano, Antarctica imaged by high-resolution active-source seismic tomography and coda interferometry. J Geophys Res Solid Earth 2013;118:1067–78. http://dx.doi.org/10.1002/jgrb.50073.